LARGE-EDDY SIMULATION OF OXYGEN TRANSFER TO ORGANIC SEDIMENT BEDS

Carlo Scalo and Ugo Piomelli
Department of Mechanical and Materials Engineering.
Queen's University,
130 Stuart Street, Kingston, Ontario, Canada
cscalo.ca@gmail.com, ugo@me.queensu.ca

Leon Boegman
Department of Civil Engineering
Queen's University
58 University Avenue, Kingston, Ontario Canada
Leon.Boegman@civil.queensu.ca

ABSTRACT

We implemented and tested a bio-geochemical model for dissolved oxygen (DO) transfer from water to underlying organic sediment beds coupled with Large-Eddy Simulation of turbulent transport on the water side. A new numerical strategy for the coupling of the discretized governing equations on both sides has been developed. The model has been tested against laboratory data. A preliminary parametric study of the sediment oxygen uptake has been performed for a range of Reynolds numbers ($Re_\tau = 180 - 1000$) and Schmidt numbers ($Sc = 200 - 500$), with an open channel model.

The mean oxygen distribution exhibits the expected behaviour for increasing wall stress: asympototic increase of the value of the mean DO concentration at the sediment-water interface (SWI), thinning of the diffusive sub-layer and increase in oxygen uptake by the organic sediment layer. We also confirm oxygen absorption trends suggested by semi-empirical transport models based on the surface-renewal theory. The effects of Sc are important at all Reynolds numbers since they affect directly the molecular DO flux at the SWI.

INTRODUCTION

The presence of dissolved oxygen (DO) is critical to the survival of aquatic life in lakes and oceans. Oxygen is absorbed by the water at the surface and transported towards the bottom by the turbulent motions. A number of physical factors can hamper this mixing process with very harmful consequences, such as oxygen depletion in the bottom layer. For instance, the stratification that occurs naturally through the water column (the water near the surface being less dense than the water at the bottom), damps the turbulent motion, reducing the supply of oxygen to the near-bed region. Here, decomposition of organic matter in the sediment layer by oxygen-consuming bacteria can cause DO concentration to drop to levels that do not allow aquatic life to survive; so called "dead zones" are, then, formed with considerable economical and environmental impacts.

Being able to predict the distribution of DO across the water column would allow a process-oriented parametrization of the SOD based on resolvable flow features in the near-wall region (such as wall shear stress). Water-quality models currently employed for lake or rivers management would considerably benefit from such parametrization. However, a full understanding of the biological responses to the thermo-fluid dynamic conditions requires physical and numerical models that couple hydro-dynamic transport and the dynamics of water quality and aquatic organisms at all the important scales (Koseff *et al.*, 1993; Boegman *et al.*, 2008*a*). These are the features incorporated in the model adopted in the present work that accounts for the characteristics of oxygen transport in a turbulent flow, transfer mechanisms the across the SWI and absorption in the sediment bed.

Oxygen transport on the water side is governed by well known conservation laws. Oxygen acts as a passive scalar with very low diffusivity (therefore, very high Schmidt numbers $Sc \gg 1$, defined as the ratio between the kinematic viscosity ν and the molecular diffusivity D) transported by a turbulent flow. On the sediment side, the most advanced biochemical DO sediment-absorption model includes a diffusive term governed by the porosity φ and a non-linear sink term (representing the oxygen absorption by decomposing organic matter in the sediments, as a non-linear function of the oxygen concentration level). One important parameter in this model is χ, the concentration of oxygen-consuming organisms, which is not directly measurable (Higashino *et al.*, 2008). Oxygen transfer from the fluid to sediments is currently modelled exclusively as a diffusive process; advection of DO in the sediment layer by pore-water flow (governed by the intrinsic permeability K) is assumed to have no effect on the mean oxygen distribution for smooth beds; however, this issue has received some attention in the literature (Higashino *et al.*, 2008, 2009).

Uncertainties also affect the determination of the value of porosity itself (Røy *et al.*, 2004; Iversen & Jørgensen, 1993). Porosity has to be obtained by calibration against experimental results, like other material properties of the sediment layer. Complete (water and sediment) measurements have been performed by O'Connor & Hondzo (2008) in a laboratory recirculating flume at different flow rates and temperatures in an attempt to correlate the sediment oxygen demand with parameters characterizing turbulent transport, like the Reynolds number or the skin-friction coefficient. The only numerical attempt, to our knowledge, to reproduce these experimental results has been with a 2D RANS transport model in a developing flat-plate boundary layer Higashino *et al.* (2008).

Although the existence of a direct dependency of the SOD on turbulence levels has been extensively demonstrated, in most water-quality models used for lake and ocean management the SOD is simply a tuneable parameter, fixed in time (and often space), and chosen over an order of magnitude scale so that DO observations can be reproduced. This is because these are RANS models, which do not resolve the spatial and temporal characteristics of the boundary layer. In Trolle *et al.* (2008) for example, the SOD is fixed to $0.7\,\mathrm{g\,m^{-2}day^{-1}}$ as a calibration parameter for a one-dimensional water-quality model applied to Lake Ravn (Denmark). In the two-dimensional model applied by Boegman *et al.* (2008*b*) to Lake Erie, SOD=$0.55\,\mathrm{g\,m^{-2}day^{-1}}$ was used. When SOD is not directly assigned a simple sediment oxygen flux model is employed that operates by assuming the flux is only a function of the overlying water temperature and dissolved oxygen concentration (*static* model) (Hipsey *et al.*, 2006). Using this model with a three-dimensional hydrodynamic driver Leon *et al.* (2011) find good agreement with measured DO profiles in Lake Erie. Such lower-level models do not capture the effect of flow dynamics and are still at an early stage of development.

In the present work we use large-eddy simulation (LES) coupled with the DO sediment absorption model proposed by Higashino *et al.* (2008) to investigate the mechanisms governing the DO transfer rate across the SWI as a function of the parameters characterizing the turbulent transport and diffusion properties of the flow such as Re_τ and Sc. In the following we begin by describing the complete model, which includes the governing equations and the numerical method for the coupling of the two layers. The comparison between the predictions of our model and the experimental results are only shown for one case, the analysis of the preliminary results of the parametric study follows.

PROBLEM FORMULATION

The filtered equations of conservation of mass and momentum can be obtained by applying a filtering operator $\overline{(\,)}$ (Leonard, 1974) to the governing equations, resulting in:

$$\frac{\partial \overline{u}_i}{\partial x_i} = 0, \tag{1}$$

$$\frac{\partial \overline{u}_j}{\partial t} + \frac{\partial \overline{u}_i \overline{u}_j}{\partial x_i} = -\frac{\partial \overline{p}}{\partial x_j} - \frac{\partial \tau_{ij}}{\partial x_i} + \frac{1}{Re_\tau}\nabla^2 \overline{u}_j - f\delta_{1i} \tag{2}$$

where x_1, x_2 and x_3 (or x, y and z) are, respectively, the streamwise, wall-normal and spanwise directions, and $\overline{u}_i$ the filtered velocity components in those directions. These equations have been made dimensionless by using δ (height of the open channel) as reference length scale, and U_b (the volume average streamwise velocity component) as velocity scale. The bulk Reynolds number is $Re_\tau = U_b\delta/\nu$; where ν is the kinematic viscosity of water. The forcing term f in the streamwise momentum equation represents the normalized mean pressure gradient driving the flow. The sub-grid scale (SGS) stresses are modelled using the plane-averaged dynamic eddy-viscosity model (Germano *et al.*, 1991; Lilly, 1992).

Oxygen dissolved in water behaves like a passive scalar. The filtered transport equation for DO is

$$\frac{\partial \overline{c}}{\partial t} + \frac{\partial \overline{u}_i \overline{c}}{\partial x_i} = \frac{\partial}{\partial x_i}\left[\frac{1}{Sc\,Re_\tau}\frac{\partial \overline{c}}{\partial x_i} - J_i^{sgs}\right] \tag{3}$$

where $Sc = \nu/D$ is the Schmidt number and $\overline{c}$ is the instantaneous filtered scalar concentration field normalized with the freestream DO concentration C_∞. The SGS scalar flux, J_i^{sgs}, is also parametrized by an eddy-diffusivity model. The extension of the dynamic model (Germano *et al.*, 1991; Lilly, 1992) to the scalar transport at high Schmidt numbers has been shown to be accurate by Zang *et al.* (1993), Calmet & Magnaudet (1997) and Na (2004).

The normalized instantaneous DO concentration level in the sediment layer, c_s, is determined by more complex mechanisms. Dissolved oxygen is diffused but also depleted by decomposing organic matter. Advection due to pore-water flow can be neglected for smooth beds. The governing equation for c_s is

$$\frac{\partial c_s}{\partial t} = \frac{\partial}{\partial x_i}\left[\frac{1}{Sc_s\,Re_\tau}\frac{\partial c_s}{\partial x_i}\right] - \dot{c_s} \tag{4}$$

where a 'sediment Schmidt number' Sc_s can be defined as $Sc_s = \nu/\varphi D_s$ (where φ is the sediment porosity and D_s is the DO molecular diffusivity in the porous medium). The DO absorption by organic matter is represented by the sink term, $\dot{c_s}$, which must be modelled.

The formulation for the DO diffusive flux used here is found in Boudreau & Jørgensen (2001). The effective diffusion coefficient inside the sediment, D_s, is lower than in water because molecules cannot travel along the concentration gradient direction but must follow a tortuous path around sediment grains. Also, the resulting flux must be reduced by a factor φ to account for the pore-space fraction available to transport in pore water. It is possible to retrieve the value of the sediment porosity (in Sc_s) from the measurable slope discontinuity in the mean oxygen profiles at the SWI (Røy *et al.*, 2004).

Following Higashino *et al.* (2008), the non-linear sink term $\dot{c_s}$ is parametrized as

$$\dot{c_s} = Re\;\mu_\chi \frac{c_s}{K_{O_2} + c_s}\chi \tag{5}$$

Table 1. Bio-geochemical parameters for oxygen absorption model (5).

μ^*_χ	$K^*_{O_2}$	Y^*_c	χ^*
2.4 day^{-1}	0.2 mg/l	1 mg$_\chi$/mg$_{DO}$	[calibrated]

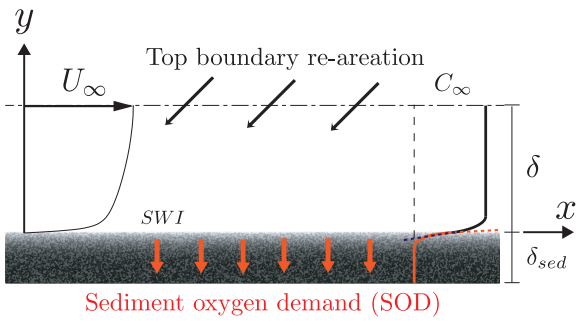

Figure 1. Computational setup. The diffusive sub-layer thickness is exaggerated for visualization purposes. The value of oxygen concentration in the bulk flow is kept at C_∞ by re-areation from top-boundary condition.

where

$$\mu_\chi = \frac{\mu^*_\chi \nu}{U_b^2}; \quad K_{O_2} = \frac{K^*_{O_2}}{C_\infty}; \quad \chi = \frac{\chi^*}{Y_c C_\infty}. \tag{6}$$

The parameters used in (6) are μ^*_χ, maximum specific DO utilization rate (in day^{-1}), $K^*_{O_2}$, half-saturation coefficient for DO utilization (in mg/l), Y_c effective yield for the microbial utilization of DO and χ^*, is the value of biomass concentration of oxygen absorbing organism, currently not directly measurable. The values of these constants are shown in Table 1. We will assume a constant and uniform value of χ^* as done by Higashino *et al.* (2008).

COMPUTATIONAL SETUP

The computational setup used is shown in Figure 1. The flow is driven by a pressure gradient $f\,\delta_{1i}$, constant in space and time. The governing equations (1), (2) and (3) are solved in a Cartesian domain. In the streamwise and spanwise directions, x and z, periodic boundary conditions are used for all quantities. The velocity obeys, at the lower wall, no-slip conditions and, at the top boundary, free-slip conditions; for the scalar we use Neumann conditions, with assigned flux. The oxygen dynamically absorbed by the sediment layer across the SWI is reinserted in the flow, at the same rate, from the top boundary by means of an imposed instantaneous flux. The value of the volume averaged DO concentration level is maintained constant and equal to the initial value.

The numerical model used to compute the flow on the water side is a well-validated finite-difference code (Keating *et al.*, 2004), based on a staggered grid. Second-order central differences are used for both convective and diffusive terms. The time advancement scheme is a Crank-Nicolson scheme for the wall-normal diffusive term, and a low-storage 3rd-order Runge-Kutta method for the other terms. The solution of the Poisson equation is obtained by Fourier transform of

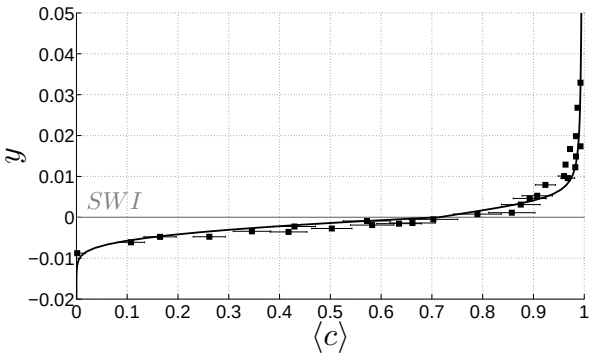

Figure 2. Comparison between the channel flow model (———) and experiments (■) for case RF3 in O'Connor & Hondzo (2008) ($Re_\tau = 360$ and $Sc = 291$). Error-bars taken from Higashino *et al.* (2008) and Røy *et al.* (2004).

the equation in the spanwise and streamwise directions, followed by a direct solution of the resulting tridiagonal matrix, at each wavenumber. The code is parallelized using the MPI protocol. The equations in the sediment layer are solved with the same numerical approach as the one adopted for water side and have the same accuracy and stability properties.

An important aspect of the present work is the coupling between the water and sediment layers. We developed a procedure that can enforce, on average, the continuity of both the DO flux and concentration profile at the SWI . Such procedure allows the implicit time-advancement of the solution in both layers (required to avoid the viscous time-step limitation caused by the highly stretched meshes near the SWI) while algebraically independent calculations are performed in the two separate computational domains (water and sediment).

We performed LES of open channel flow by adjusting the forcing term in (2) in order to obtain four different friction Reynolds numbers $Re_\tau = 180,\ 400,\ 600$ and 1000. Each calculation has been repeated for two Schmidt numbers $Sc = 200$ and 500. The box size has been chosen in order to accommodate the large structures and the near-wall streaks. The grid size has been chosen accordingly in order to keep the resolution constant in all cases at $\Delta x^+ \simeq 25$ and $\Delta z^+ \simeq 13$. The resolution in the wall normal direction depends on the diffusive sub-layer thickness δ_s that can be estimated based on the Sc and Re_τ. In all cases the sediment layer depth is fixed to $\delta_{sed} = .3\delta$, with $\delta = 10cm$. All the parameters used are summarized in Table 2 and 3.

Table 2. Summary of LES parameters.

Re_τ	Box size	Grid Size	Sc
180	$16 \times 1 \times 8$	$128 \times 128 \times 128$	200, 500
400	$7 \times 1 \times 3.5$	$128 \times 128 \times 128$	200, 500
600	$7 \times 1 \times 3.5$	$192 \times 192 \times 192$	200, 500
1000	$7 \times 1 \times 3.5$	$256 \times 192 \times 256$	200, 500

Table 3. Summary of fluid and sediment properties used in LES. Correspondent values of u_τ and D for each case in Table 2 can be obtained from $u_\tau = Re_\tau \nu/\delta$ and $D = \nu/Sc$.

φ	ν	C_∞	χ^*
0.8	0.89×10^{-6} m^2/s	6 mg/l	700 mg/l

RESULTS

First, we verified that good agreement was found between first and second order velocity field statistics of our LES and reference DNS data at comparable Reynolds numbers (Kim *et al.*, 1987; Moser *et al.*, 1999; Hoyas & Jiménez, 2008). Also, a grid convergence test was carried out to asses the dependence of the predicted first and second order scalar statistics to the grid resolution for Neumann boundary conditions in a channel flow for $Re_\tau = 400$ and $Sc = 10-300$ (not shown). Mean profiles and total turbulent flux profiles converge even on coarse grids, provided the diffusive sub-layer is resolved. A slight grid dependency can still be observed in the scalar variance profiles which collapse, for every grid, over the more than 99 % of the channel height, varying only in part of the diffusive sub-layer (by 5 % in the last refinement step).

The predictions of our complete oxygen transport and absorption model have been compared against experimental results reported by O'Connor & Hondzo (2008) for validation purposes. We report in Figure 2 the comparison between experimental data and LES predictions only for case RF3 in the paper, corresponding to $Re_\tau = 360$ and $Sc = 291$. Excellent agreement is observed for calibrated porosity and bacterial population of $\varphi = .63$ and $\chi^* = 700$ mg/l. Good agreement is also found for lower Reynolds numbers investigated in the experiments. However, for higher Reynolds numbers the quality of the agreement begins to deteriorate. The discussion of the observed discrepancy can be attributed to uncertainties in the determination of the sediment properties (Scalo *et al.*, 2011).

In Figure 3 mean DO profiles for all cases investigated are shown. Lower Sc result in more intense molecular transport causing, for a given Re_τ, the thickening of the diffusive sub-layer on the water side and larger penetration depths on the sediment side. Also, the mean value of oxygen at the SWI increases for lower Sc as the (diffusive) flux of oxygen from the water side to the sediment becomes stronger. On the other hand, increasing Re_τ results in a thinner viscous sub-layer, and, therefore, a thinner diffusive sub-layer. This also increases the magnitude of the diffusive flux of oxygen across the SWI, the DO uptake by the sediment layer and the value of DO at the SWI. A rather low sensitivity of the penetration depth to changes in the wall shear stress is observed; changes in Schmidt number, on the other hand, have a pronounced effect on both sides of the SWI.

The control of the oxygen uptake is a function of momentum and scalar transport. As the Reynolds number increases, for fixed sediment characteristics, the SOD approaches its potential value (the sediment saturation limit), or PSOD. This is observed in the increase in mean DO concentration at the SWI, C_{swi}, whose changes become smaller as Re_τ increases, for any given Sc . The non-linear term in (5) controls the

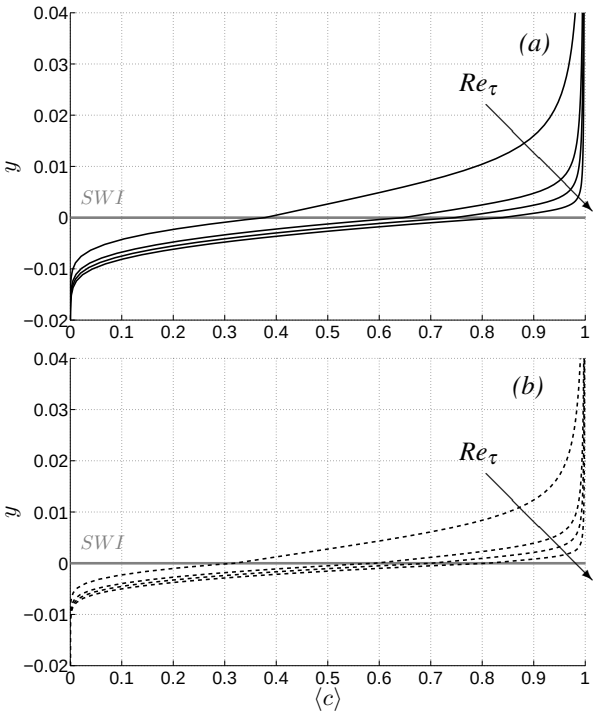

Figure 3. Mean oxygen concentration profiles for $Sc = 200$ *(a)* and for $Sc = 500$ *(b)*. Arrows show the direction of increasing Reynolds number for $Re_\tau = 180,\ 400,\ 600$ and 1000.

growth of the value of C_{swi} since its intensity grows monotonically as the DO level in the sediments tends toward the saturation limit.

The parametrization of J_{swi}, with respect to Sc and Re_τ, is typically formulated considering the Sherwood number, a normalized form of J_{swi}, defined as

$$Sh = \frac{Re_\tau Sc}{1-C_{swi}} J_{swi}. \tag{7}$$

Based on a semi-empirical model, derived from the surface-renewal theory (Boudreau & Jørgensen, 2001; O'Connor & Hondzo, 2008), the relationship $Sc = f(Re_\tau, Sc)$ takes on the form

$$Sh = \frac{.807}{(a_1/2)^{1/3}} Re_\tau Sc^{1/3} \tag{8}$$

shown in Figure 4 for $a_1 = 238.5$ (value taken from O'Connor & Hondzo (2008)) along with our LES results in terms of Re_τ. Values of the dimensionless scaling constant a_1 (related to the average period between bursting events) can lie between 200 and 300 (Pinczewski & Sideman, 1974). Predictions from the semi-empirical model show a systematic over-estimation of the DO flux with respect to the LES results. However, the derivation of such model, does not take into account the contribution of the sink term (5) that tends to decrease the value of C_{swi} (increase $(1-C_{swi})$ in (7)) with respect to a non-organic porous boundary.

Instantaneous visualizations of the spatial distribution of J_{swi} (Figure 5) reveal very fine and organized structures at the

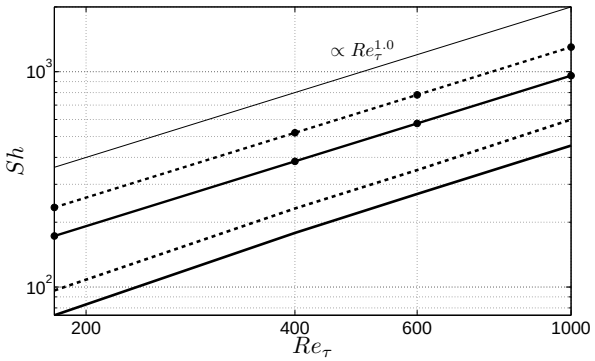

Figure 4. Sherwood number Sh plotted against friction Reynolds number Re_τ. Results are for $Sc = 200$ (solid line) and $Sc = 500$ (dashed line). Correspondent predictions of the relation (8) for $a_1 = 238.5$ are shown for $Sc = 200$ (solid line with filled circles) and $Sc = 500$ (dashed line with filled circles).

SWI, that are characteristic of the water-side transport dynamics. The signature of bursting events, which govern the transport of momentum and scalar concentration in the turbulent core, may still be detected across most of the diffusive sub-layer thickness, as found by Dworak & Wendt (1977) in high-Sc-number fluids. Also, the build-up process of the viscous sub-layer, after a sweep event, occurs on a much shorter time scale then the successive relaxation of the diffusive sub-layer. This is shown by comparing the time autocorrelation functions (not shown here) of the wall shear stress τ_w, C_{swi} and J_{swi}. The integral time scale associated with the momentum turbulent transport is, approximately, 6 times smaller than the time scales associated with the oxygen fluctuations and flux at the SWI. Increasing the Schmidt number further increases this time scale separation. However, the time evolution of these three quantities is statistically correlated by the near-wall transport dynamics. The time cross-correlations in Figure 6 give insight of near-wall transport mechanisms of oxygen transfer and depletion to organic sediments; sweep events, that cause instantaneous increase of τ_w, are followed by a corresponding increase of J_{swi}, probably due to the thinning of the diffusive sub-layer, with a well defined time lag (Figure 6 *(b)*); the increased J_{swi} causes an instantaneous excess of DO supply to the sediment layer (controlled by the sink term (5)) which causes a sudden increase in C_{swi}, with another time lag (Figure 6 *(c)*); the aforementioned time lags are roughly cumulated when looking at the overall cross correlation between τ_w and C_{swi} (Figure 6 *(a)*). The time lag between these events is emphasized for the higher Sc case, consistently with what previously observed.

CONCLUSIONS

We implemented and tested an existing bio-geochemical model for dissolved oxygen (DO) transfer from water to underlying organic sediment beds coupled with Large-Eddy Simulation (LES) of turbulent transport on the water side. In a preliminary validation phase results have been compared with experimental data and self-consistency of the numerical model has been assessed with grid convergence tests.

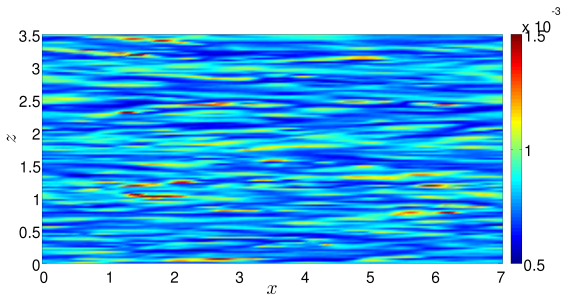

Figure 5. Contour plot of diffusive flux J_{swi} at SWI for $Re_\tau = 400$ and $Sc = 200$.

We have discussed the relation between the wall shear stress and the SOD. For $180 < Re_\tau < 1000$ the parameters characterizing the oxygen transfer to sediment layer, such as diffusive sub-layer thickness, penetration depth, and, most remarkably, the SOD and oxygen concentration at SWI interface, seem to asymptote towards a prescribed value in the limit $Re_\tau \to \infty$. The dependency from the Schmidt number (oxygen diffusivity) is very pronounced at all Re_τ. The semi-empirical law for mass transfer at high Schmidt numbers based on the surface-renewal theory is only confirmed qualitatively. Time correlations at the SWI give a first picture of the near-wall transport dynamics revealing, among other things, a well-defined time lag between the re-establishment of the diffusive sub-layer after bursting events.

REFERENCES

Boegman, L., Loewen, M.R., Hamblin, P.F. & Culver, D.A. 2008*a* Vertical mixing and weak stratification over zebra mussel colonies in western Lake Erie. *Limnol. Oceanogr.* **53** (3), 1093–1110.

Boegman, L., Loewen, M. R., Culver, D. A., Hamblin, P. F. & Charlton, M. N. 2008*b* Spatial-Dynamic Modeling of Algal Biomass in Lake Erie: Relative Impacts of Dreissenid Mussels and Nutrient Loads. *J. Environ. Eng-ASCE* **134** (6), 456–468.

Boudreau, B.P. & Jørgensen, B.B. 2001 *The Benthic Boundary Layer: Transport Processes and Biogeochemistry*. Oxford University Press, New York.

Calmet, I. & Magnaudet, J. 1997 Large-eddy simulation of high-schmidt number mass transfer in a turbulent channel flow. *Phys. Fluids* **9**, 438.

Dworak, R. & Wendt, H. 1977 Stochastic fluctuations of mass transport through turbulent boundary layers. *Berichte der Bunsengesellschaft für physikalische Chemie* **81** (9), 864–869.

Germano, M., Piomelli, U., Moin, P. & Cabot, W.H. 1991 A dynamic subgrid-scale eddy viscosity model. *Phys. Fluids A* **3**, 1760–1765.

Higashino, M., Clark, J.J. & Stefan, H.G. 2009 Pore water flow due to near-bed turbulence and associated solute transfer in a stream or lake sediment bed. *Water Resour. Res.* **45** (12), W12414.

Higashino, M., O'Connor, B. L., Hondzo, M. & Stefan, H. G.

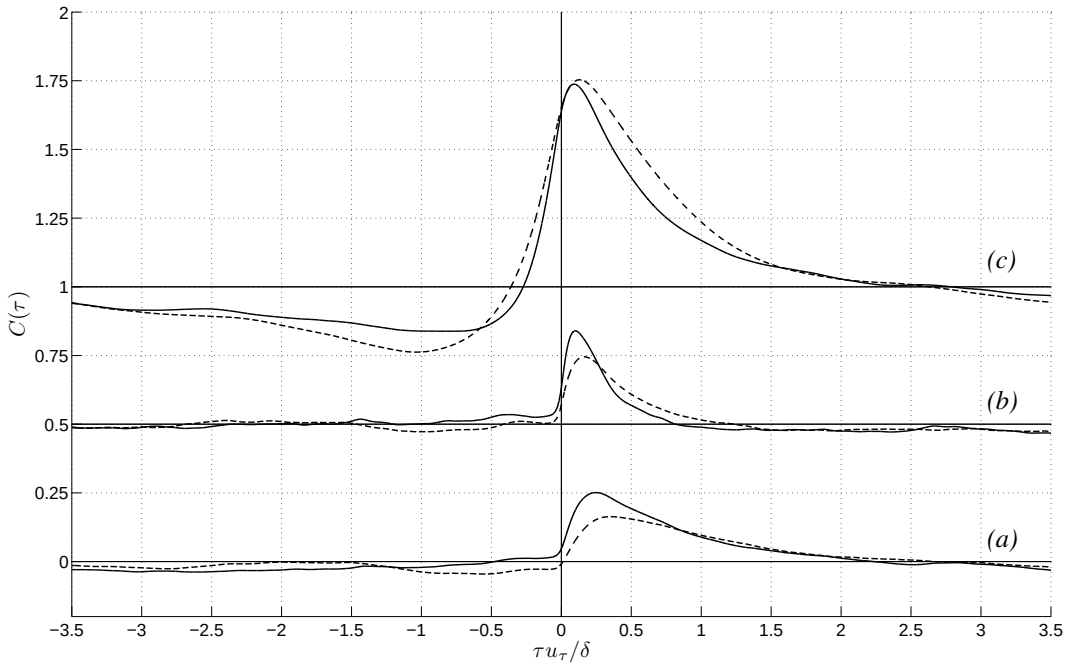

Figure 6. Cross-correlation coefficient $C(\tau)$ for $Re_\tau = 400$ between τ_w and C_{swi} *(a)*, τ_w and J_{swi} *(b)* and J_{swi} and C_{swi} *(c)*, for $Sc = 200$ (solid line) and $Sc = 500$ (dashed line). Note that the cross-correlation coefficients have been shifted by 0.5 for clarity.

2008 Oxygen transfer from flowing water to microbes in an organic sediment bed. *Hydrobiologia* **614**, 219–231.

Hipsey, M.R., Romero, J.R., Antenucci, J.P. & Hamilton, D. 2006 *The Computational Aquatic Ecosystem Dynamics Model (CAEDYM): v3.1*. Centre for Water Research, Perth, Australia.

Hoyas, S. & Jiménez, J. 2008 Reynolds number effects on the Reynolds-stress budgets in turbulent channels. *Phys. Fluids* **20**, 101511.

Iversen, N. & Jørgensen, B.B. 1993 Diffusion coefficients of sulfate and methane in marine sediments: Influence of porosity. *Geochim. Cosmochim. Ac.* **57** (3), 571–578.

Keating, A., Piomelli, U., Bremhorst, K. & Nešić, S. 2004 Large-eddy simulation of heat transfer downstream of a backward-facing step. *J. Turbul.* **5** (20), 1–27.

Kim, J., Moin, P. & Moser, R. 1987 Turbulence statistics in fully developed channel flow at low Reynolds number. *J. Fluid Mech.* **177**, 133–166.

Koseff, J.R., Holen, J.K., Monismith, S.G. & Cloern, J.E. 1993 Coupled effects of vertical mixing and benthic grazing on phytoplankton populations in shallow, turbid estuaries. *J. Mar. Res.* **51** (4), 843–868.

Leon, Luis F., Smith, Ralph E.H., Hipsey, Matthew R., Bocaniov, Serghei A., Higgins, Scott N., Hecky, Robert E., Antenucci, Jason P., Imberger, Jorg A. & Guildford, Stephanie J. 2011 Application of a 3d hydrodynamic-biological model for seasonal and spatial dynamics of water quality and phytoplankton in lake erie. *Journal of Great Lakes Research* **37** (1), 41–53.

Leonard, A. 1974 Energy cascade in large-eddy simulations of turbulent fluid flows. *Adv. Geophys.* **18**, 237–248.

Lilly, D. K. 1992 A proposed modification of the germano subgrid-scale closure method. *Phys. Fluids A* **4**, 633–635.

Moser, R.D., Kim, J. & Mansour, N.N. 1999 Direct numerical simulation of turbulent channel flow up to Re = 590. *Phys. Fluids* **11**, 943.

Na, Y. 2004 On the large-eddy simulation of high Prandtl number scalar transport using dynamic subgrid-scale model. *J. Mech. Sci. Technol.* **18** (1), 173–182.

O'Connor, B. L. & Hondzo, M. 2008 Dissolved oxygen transfer to sediments by sweep and eject motions in aquatic environments. *Limnol. Oceanogr.* **53** (2), 566–578.

Pinczewski, WV & Sideman, S. 1974 A model for mass (heat) transfer in turbulent tube flow. Moderate and high Schmidt (Prandtl) numbers. *Chemical engineering science* **29** (9), 1969–1976.

Røy, H., Huettel, M. & Joergensen, B. B. 2004 Transmission of oxygen concentration fluctuations through the diffusive boundary layer overlying aquatic sediments. *Limnol. Oceanogr.* **49** (3), 686–692.

Scalo, C., Piomelli, U. & Boegman, L. 2011 Large-eddy simulation of oxygen transfer to organic sediment beds. Submitted to J. Geophys. Res.

Trolle, D., Skovgaard, H. & Jeppesen, E. 2008 The Water Framework Directive: Setting the phosphorus loading target for a deep lake in Denmark using the 1D lake ecosystem model DYRESM-CAEDYM. *Ecol. Model.* **219** (1-2), 138–152.

Zang, Y., Street, R.L. & Koseff, J.R. 1993 A dynamic mixed subgrid-scale model and its application to turbulent recirculating flows. *Phys. Fluids A-Fluid* **5**, 3186.